IEEE Photonics Journal
An IEEE Photonics Society Publication

Open Access

Simultaneous Generation of Multi-Channel Broadband Chaotic Signals Based on Two Unidirectionally Coupled WRC-FPLDs

Volume 12, Number 5, October 2020

Chun-Xia Hu
Guang-Qiong Xia
Zai-Fu Jiang
Dian-Zuo Yue
Wen-Yan Yang
Gong-Ru Lin
Zheng-Mao Wu

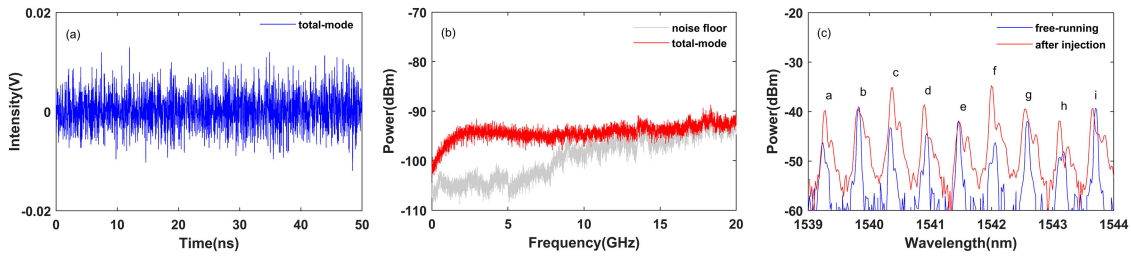

DOI: 10.1109/JPHOT.2020.3027598

Simultaneous Generation of Multi-Channel Broadband Chaotic Signals Based on Two Unidirectionally Coupled WRC-FPLDs

Chun-Xia Hu,[1,2] Guang-Qiong Xia,[1] Zai-Fu Jiang,[1] Dian-Zuo Yue,[1] Wen-Yan Yang,[1,3] Gong-Ru Lin,[4] and Zheng-Mao Wu[1]

[1]School of Physical Science and Technology, Southwest University, Chongqing 400715, China
[2]College of Mobile Telecommunications, Chongqing University of Posts and Telecom, Chongqing 401520, China
[3]School of Mathematics and Physics, Chongqing University of Science and Technology, Chongqing 401331, China
[4]Graduate Institute of Photonics and Optoelectronics, National Taiwan University, Taipei 10617, Taiwan

DOI:10.1109/JPHOT.2020.3027598

Manuscript received August 21, 2020; accepted September 25, 2020. Date of publication September 29, 2020; date of current version October 16, 2020. This work was supported by the National Natural Science Foundation of China under Grants 61775184 and 61875167. Corresponding authors: Guang-Qiong Xia; Gong-Ru Lin; Zheng-Mao Wu. (e-mail: gqxia@swu.edu.cn; grlin@ntu.edu.tw; zmwu@swu.edu.cn).

Abstract: We propose and demonstrate experimentally a scheme for simultaneously generating multi-channel broadband chaotic signals based on two unidirectionally coupled weak-resonant-cavity Fabry-Perot laser diodes (WRC-FPLDs) with almost the same mode interval, where one WRC-FPLD is utilized as master WRC-FPLD (M-WRC-FPLD) and the other is used as slave WRC-FPLD (S-WRC-FPLD). Under the optical injection from the M-WRC-FPLD with suitable injection parameters, multiple longitudinal modes of the S-WRC-FPLD can be simultaneously driven into chaotic states, which can provide multi-channel chaotic signals. Via a tunable optical filter, we inspect the performances of 9-channel chaotic signals, the results show that the chaotic bandwidths are within the range of 8∼15 GHz for all the 9-channel chaotic signals. Furthermore, the influences of the injection power and frequency detuning on the performances of the chaotic output from one of the channels are also analyzed.

Index Terms: Multi-channel chaotic signal, unidirectional coupling, weak resonant-cavity Fabry-Perot laser diodes (WRC-FPLD).

1. Introduction

For years, optical chaos has been paid much attention due to its potential applications in various fields including physical random bit generation [1]–[3], optical time domain reflectometers (OTDR) [4], ranging lidars [5]–[7], and chaos-based optical communications [8]–[14]. In general, optical chaotic signal can be relatively easily generated by using a semiconductor laser (SL) under external

disturbances such as optical injection [15]–[17], optical feedback [18]–[20] and optoelectronic feedback [21]–[23]. Considering that some application scenarios need multi-channel chaotic signals, several SL-based schemes for generating multi-channel chaotic signals are proposed and related applications of multi-channel chaotic signals are demonstrated [24]–[30]. For instance, based on two single-mode SLs, Paul *et al.* proposed a scheme for generating dual-channel chaotic signals, which are utilized as two chaotic carriers for achieving dual-channel chaotic optical communication [24]. Based on two mutually coupled DFB-SLs, Tang *et al.* demonstrated the generation of dual-channel chaotic signals, which are taken as the chaotic entropy source to generate high-speed physical random bits [25]. Via a ring network composed of three mutually coupled DFB-SLs, Xiang *et al.* proved that the three DFB-SLs can output three chaotic signals. Through further combining the three chaotic signals, it can be obtained seven channels of chaotic entropy sources. As a result, seven channel physical random bit sequences can be simultaneously generated [26]. Different from DFB-SLs, vertical-cavity surface-emitting lasers (VCSELs) may support two orthogonal polarization components co-existing in the cavity. As a result, VCSELs can output two chaotic signals under suitable operation condition. Based on two mutually coupled VCSELs, our group demonstrated that four-channel chaotic signals can be generated. Taking the four-channel chaotic signals as chaotic entropy sources, four-channel physical random bit sequences are obtained [27]. Even so, the channel number of the chaotic signals generated by DFB- SLs or VCSELs is limited by the characteristics of the two types of SLs.

Compared with DFB-SLs and VCSELs, Fabry-Perot laser diodes (FPLDs) possess a unique potential to generate multi-channel chaotic signals due to multi-longitudinal modes co-existing in the cavity. Jiang *et al.* theoretically demonstrated that the multi-longitudinal modes can be simultaneously driven into chaotic states, and a physically enhanced secure wavelength division multiplexing (WDM) chaos communication scheme is hopeful for achieving [28]. Based on a FPLD, Li *et al.* experimentally reported the generation of 19-channel chaotic signals with relative flat power spectra [29]. Compared with conventional FPLDs, weak-resonant-cavity Fabry-Perot laser diodes (WRC-FPLDs) possess broader gain spectra and smaller longitudinal mode interval due to lower front-end reflectivity and longer cavity length [31]–[34]. As a result, much more longitudinal modes can be stimulated in a WRC-FPLD. In Ref. [33], our group demonstrated that a WRC-FPLD can output a chaotic signal with tunable central wavelength after introducing filtered optical feedback. Under this case, in the WRC-FPLD, only one longitudinal mode oscillates and behaves chaotic state. Through adjust the filtered optical feedback, different longitudinal mode can be selected to oscillate, and then the central wavelength of the chaotic output can be tuned. Although this scheme reported in Ref. [33] can be utilized to generate a chaotic signal with tunable central wavelength, only one longitudinal mode output limits its multi-channel related applications. In fact, the simultaneous generation of multi-channel chaotic signals has potential applications in WDM chaos secure commination, multi-channel chaos lidar, multi-channel physical random number acquisition and other multi-channel related fields. Based on above considerations, in this work, we focus on the generation of multiple-channel chaotic signals based on WRC-FPLDs. Via two unidirectional coupled WRC-FPLDs, a simple scheme for simultaneously generating multi-channel broadband chaotic signals is proposed, and the performances of the generated multi-channel broadband chaotic signals are investigated experimentally. In such a scheme, a free-running WRC-FPLD is utilized as master WRC-FPLD (M-WRC-FPLD), its output of multiple longitudinal modes is injected into the other WRC-FPLD named as slave WRC-FPLD (S-WRC-FPLD). Under suitable injection condition, about 40 longitudinal modes (within 10 dB amplitude variation) of the S-WRC-FPLD can be simultaneously driven into chaotic states. Via a tunable optical filter, the performances of 9-channel chaotic signals are specified.

2. Experimental Setup

Figure 1 is a schematic diagram of experimental setup for generating multi-channel broadband chaotic signals based on two unidirectionally coupled WRC-FPLDs. M-WRC-FPLD and S-WRC-FPLD are driven by high-precision and low-noise current sources (ILX-Lightwave, LDC-3724C).

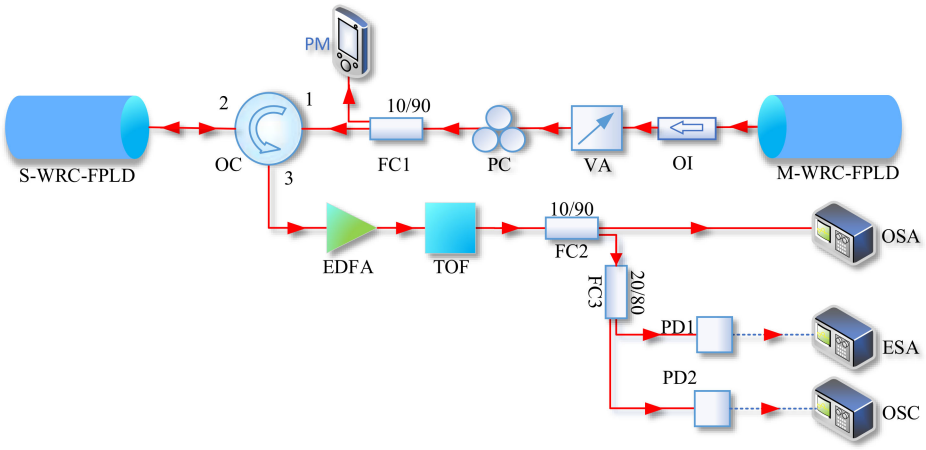

Fig. 1. Experimental setup for generating multi-channel chaotic signals based on two unidirectionally coupled WRC-FPLDs. M-WRC-FPLD: master weak-resonant-cavity Fabry-Perot laser diode; S-WRC-FPLD: slave weak-resonant-cavity Fabry-Perot laser diode; OI: optical isolator; VA: variable optical attenuator; PC: polarization controller; FC1, FC2, FC3: optical coupler; OC: optical circulator; EDFA: erbium-doped fiber amplifier; TOF: tunable optical filter; OSA: optical spectrum analyzer; PD: photodetector; ESA: electrical spectrum analyzer; OSC: digital oscilloscope.

The output light of M-WRC-FPLD passes through an optical isolator, a variable attenuator (VA) and a polarization controller (PC), and then is split into two parts by a 10:90 fiber coupler (FC1). The 10% part is sent to an optical power meter (PM, Thorlabs PM100D) for monitoring the optical power injected into the S-WRC-FPLD, and the other 90% part is injected into the S-WRC-FPLD through port 1 of an optical circulator (OC). The output light of the S-WRC-FPLD is amplified by an erbium-doped fiber amplifier (EDFA), and then filtered by a tunable optical filter (TOF, EXFO XTM-50). The filtered signal is split into two parts by a 10:90 FC2, where 10% output enters an optical spectrum analyzer (OSA, Ando AQ6317C) for recording optical spectrum and 90% output is divided into two parts by a 20:80 FC3. The 80% output from FC3 is converted into an electrical signal by a photodetector (PD1, Finisar XPDV2120R, 50 GHz bandwidth), and then enters an electronic spectrum analyzer (ESA, Rohde & Schwarz FSW67) for power spectrum measurement. The other 20% output from FC3 is used to record the time series by a digital oscilloscope (OSC, Agilent X91604A) after converted into electrical signal by a photodetector (PD2, New Focus 1544-B, 12 GHz bandwidth).

3. Results and Discussion

During the entire experiment, the currents of S-WRC-FPLD and M-WRC-FPLD are biased at 29.51 mA and 27.93 mA, respectively. The temperature of the S-WRC-FPLD is fixed at 17.31 °C, under which the threshold current of the S-WRC-FPLD is 22.05 mA. Figure 2(a) shows the optical spectrum of the free-running M-WRC-FPLD, where the laser temperature is set at 19.30 °C and its threshold current is 26.85 mA. From this diagram, one can see that there are 62 longitudinal modes within the C-band (1530 nm-1565 nm), and the mode interval is about 0.56 nm. Figure 2(b) shows the optical spectrum of the free-running S-WRC-FPLD. Similarly, there are also 62 longitudinal modes in the C-band with the mode interval of about 0.56 nm. Due to the almost same mode interval for the two lasers, the frequency detuning between two corresponding longitudinal modes of the two lasers is almost identical. As a result, the frequency detuning Δf can be defined as $\Delta f = f_k{}^m - f_k{}^s$, where $f_k{}^m$ and $f_k{}^s$ are the k-th longitudinal mode frequency of the free-running M-WRC-FPLD and S-WRC-FPLD, respectively. Under above operation conditions, $\Delta f = 1$ GHz. In fact, the value of Δf can be adjusted through changing the temperature of the M-WRC-FPLD, meanwhile the injection

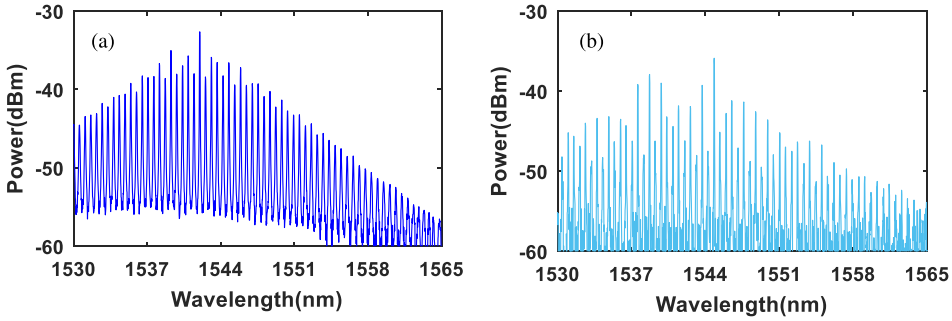

Fig. 2. (a) Optical spectrum of free-running M-WRC-FPLD under the current of 27.93 mA and the temperature of 19.30 °C; (b) Optical spectrum of free-running S-WRC-FPLD under the current of 29.51 mA and the temperature of 17.31 °C.

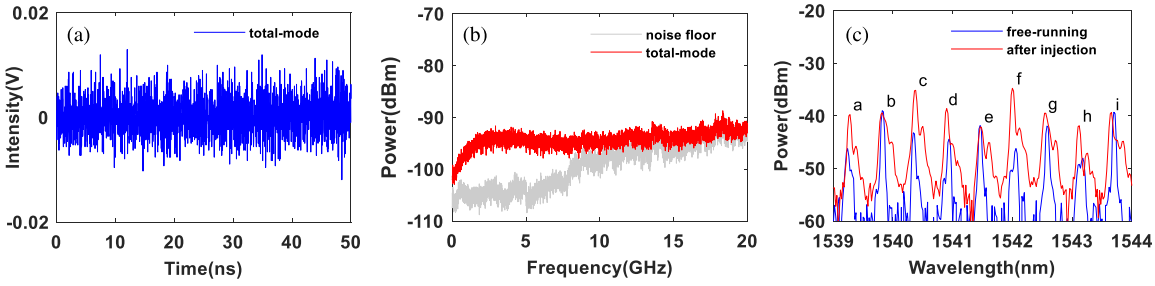

Fig. 3. Time series (a), power spectrum (b), and optical spectrum (c) of the total chaotic output from S-WRC-FPLD under optical injection with the injection power of $P_{\rm in} = 276.04\ \mu$W and the frequency detuning of $\Delta f = 1$ GHz. The gray line in power spectra denotes the noise floor.

power can also be controlled via the VA. Thus, the dynamic characteristics of the S-WRC-FPLD under optical injection with different Δf and injection power can be investigated.

First, we examine the total output characteristics of the S-WRC-FPLD under optical injection from the M-WRC-FPLD, where the operating parameters are the same as that used to obtain Fig. 2. It should be pointed out that, in order to measure the total output from the S-WRC-FPLD, the TOF in the system setup (as shown in Fig. 1) needs to be removed. Figure 3 displays the time series (a) and power spectrum (b) of the total chaotic output from the S-WRC-FPLD under the optical injection with the injection power of $P_{\rm in} = 276.04\ \mu$W and the frequency detuning of $\Delta f = 1$ GHz. The time series fluctuates dramatically and irregularly, and meanwhile the power spectrum is continuous. Moreover, the optical spectrum for each longitudinal mode is significantly broadened. About 40 longitudinal modes within the 10 dB amplitude variation of the S-WRC-FPLD can be simultaneously driven into chaotic states, where partial optical spectrum is given in Fig. 3(c). As shown in Fig. 2, the longitudinal modes located within 1539 nm to 1544 nm possess relative strong output power, and therefore we only concern the longitudinal modes located within such a wavelength range. There exist 9 longitudinal modes within 1539 nm to 1544 nm, which are marked with letters from “a” to “i”, respectively. Based on above output performances, it can be deduced that the S-WRC-FPLD is operating at chaotic state. Additionally, from Fig. 3(b), one can find that most of the energy of the total chaotic output is concentrated around the laser relaxation oscillation frequency (about 3 GHz), and the low frequency part gets less energy.

Next, via a TOF to filter out a specific longitudinal mode, the characteristic of the longitudinal mode can be analyzed. Through adjusting the central wavelength of the TOF to be identical with the peak wavelength of a special longitudinal mode, the special longitudinal mode can be extracted. Considering the mode interval of the laser is 0.56 nm, we fix the 3 dB bandwidth of the TOF at

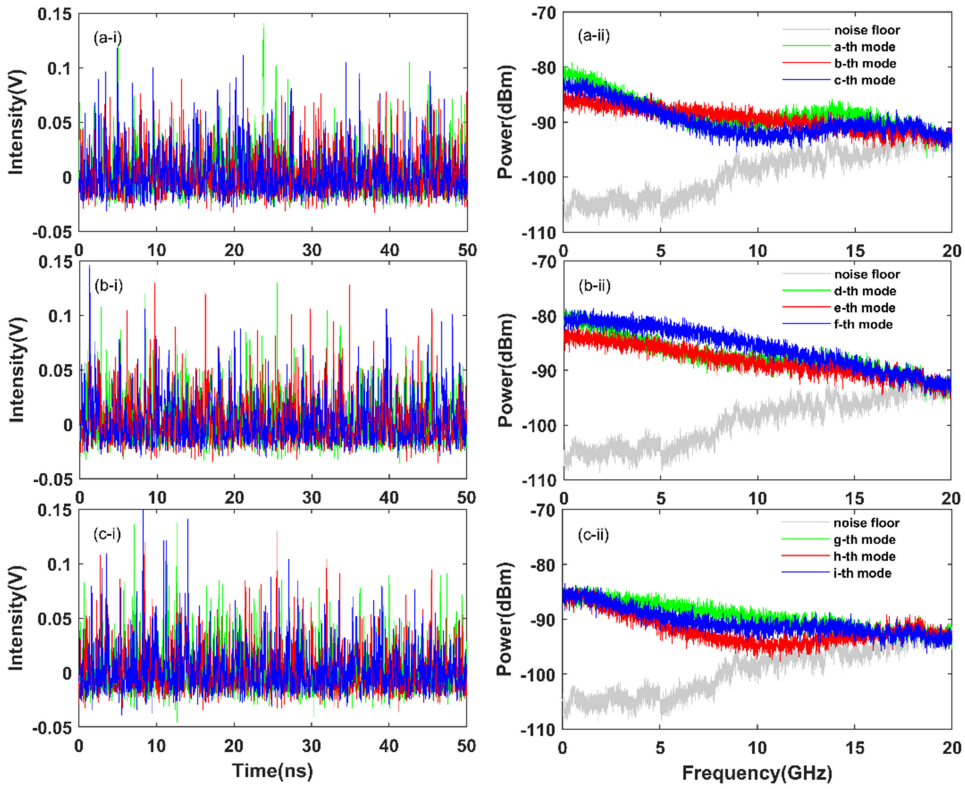

Fig. 4. Time series (left column) and power spectra (right column) of the output from the S-WRC-FPLD under optical injection with $\Delta f = 1$ GHz and $P_{\rm in} = 276.04$ μW, where the first row is for a-th∼c-th mode, the second row is for d-th∼f-th mode, and the third row is for g-th∼i-th mode. The gray lines in power spectra denote the noise floor.

0.28 nm. Figure 4 shows the time series (left column) and power spectra (right column) of the 9 modes marked in Fig. 3(c). Obviously, the signal of each channel is still chaotic. Compared with the power spectrum of the total chaotic output (Fig. 3(b)), the energy located at the low-frequency region for each channel is stronger significantly. Taking the power spectrum of the a-th mode chaotic signal as a specific example, the energy within the low-frequency region is 20 dB higher than that of the total chaotic output (Fig. 3(b)). The reason leading to the phenomenon may be explained as follows. Due to mode competition, some modes behave anti-correlation. For two modes with anti-correlation are superimposed, the power will be deficient at low frequencies. As a result, for the total chaotic signal which is the superposition of all the longitudinal modes, the power within low frequency region will behave lower than that for a single mode [29]. The above results are obtained under $\Delta f = 1$ GHz and $P_{\rm in} = 276.04$ μW. We have further experimentally checked the case that Δf is fixed at 1 GHz and $P_{\rm in}$ is scanned. The results show that the S-WRC-FPLD operates at a periodic oscillation for $P_{\rm in} < 192.30$ μW, a chaotic state for 192.30 μW $\leq P_{\rm in} \leq 276.04$ μW, and an injection-locked state for $P_{\rm in} > 276.04$ μW, respectively. Besides the injection power, Δf is another important injection parameter affecting the dynamic characteristics of the S-WRC-FPLD. The experimental results also show that, for Δf is set within the range between -30 GHz and 30 GHz, the S-WRC-FPLD can always realize the chaotic output under suitable injection powers.

Then, taking into account that the bandwidth is an important indicator for a chaotic signal, we record the bandwidths of above 9-channel chaotic signals under different injection parameters, which are presented in Fig. 5. Here, the bandwidth of chaotic signal is defined as the span between the DC and the frequency where 80% of the energy is contained [21]. From this diagram, it can

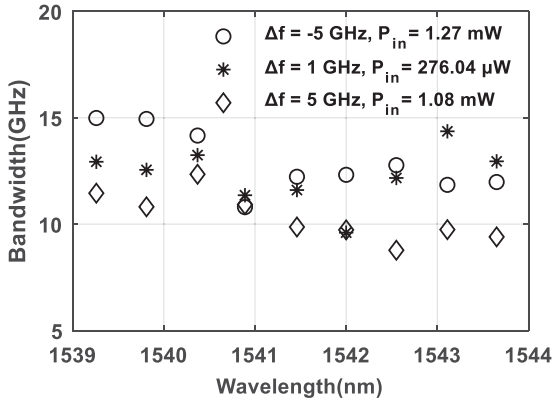

Fig. 5. Chaotic bandwidths for different channel chaotic signals output from the S-WRC-FPLD under optical injection with different injection parameters, where $\Delta f = -5$ GHz and $P_{\rm in} = 1.27$ mW (circle), $\Delta f = 1$ GHz and $P_{\rm in} = 276.04$ μW (star), $\Delta f = 5$ GHz and $P_{\rm in} = 1.08$ mW (rhombuse).

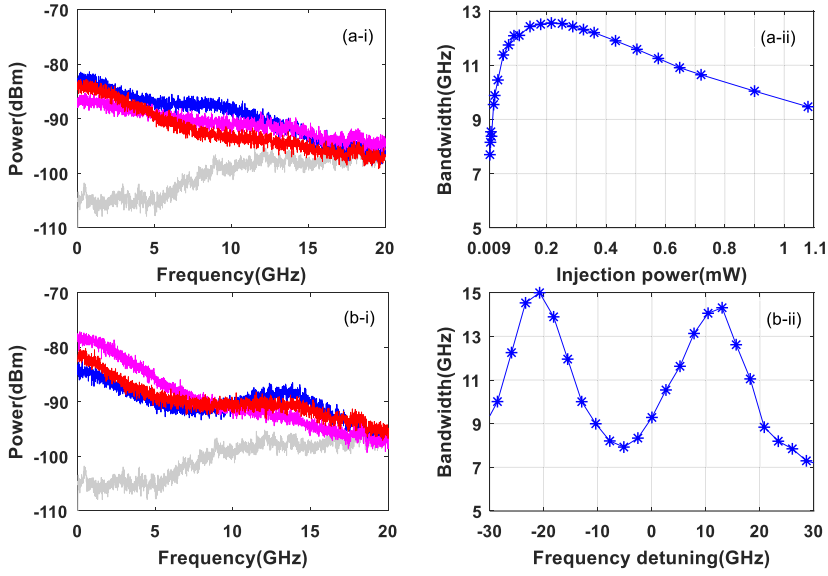

Fig. 6. (a-i) Power spectra of the i-th mode chaotic output under $\Delta f = 5$ GHz and different $P_{\rm in}$; (a-ii) Chaotic bandwidth as a function of $P_{\rm in}$ under $\Delta f = 5$ GHz; (b-i) Power spectra of the i-th mode chaotic output under $P_{\rm in} = 0.054$ mW and different Δf; and (b-ii) chaotic bandwidth as a function of Δf, under $P_{\rm in} = 0.054$ mW. The gray lines in power spectra denote the noise floor.

be seen that, under a given injection condition, there exist slightly different for the bandwidths of the 9-channel chaotic signals. Under $\Delta f = -5$ GHz and $P_{\rm in} = 1.27$ mW (circle), the bandwidths of the 9-channel chaotic signals fluctuate within the range of 10.8 GHz and 15.0 GHz. For $\Delta f = 1$ GHz and $P_{\rm in} = 276.04$ μW (star), the bandwidths of the 9-channel chaotic signals locate within the range of 9.6 GHz$\sim$14.6 GHz. For $\Delta f = 5$ GHz and $P_{\rm in} = 1.08$ mW (rhombuse), the fluctuation of the bandwidths for the 9-channel chaotic signals is relatively small within the range of 8.8 GHz$\sim$12.3 GHz.

Finally, we take the chaotic output of i-th mode as an example to clarify the impact of injection parameters on the chaotic bandwidth. For a fixed Δf of 5 GHz, the power spectra of the chaotic out under three different injection power are shown in Fig. 6(a-i). Obviously, under different injection power, the flatness of the power spectrum is different, and therefore the bandwidths of the chaotic

outputs are different from each other. In Fig. 6(a-ii), we give the dependence of the chaotic bandwidth on the injection power $P_{\rm in}$ under $\Delta f = 5$ GHz. As shown in Fig. 6(a-ii), with the increase of $P_{\rm in}$, the bandwidth increases rapidly and reaches its maximum (12.6 GHz) under $P_{\rm in} = 0.180$ mW, and then it slowly declines as $P_{\rm in}$ further increases. For a fixed $P_{\rm in}$ of 0.054 mW, the power spectra of the chaotic output under three different frequency detuning are shown in Fig. 6(b-i). For different frequency detuning, the distributions of power spectra are different, and then it can be predicted that the chaotic bandwidth should be influenced by the frequency detuning. The variation of the chaotic bandwidth with the frequency detuning Δf under $P_{\rm in} = 0.054$ mW is shown in Fig. 6(b-ii). It can be seen that the variation of the chaotic bandwidth presents an approximately symmetrical m-shaped distribution for Δf varied within -30 GHz to 30 GHz. Two maximum 15.0 GHz and 14.3 GHz are located at $\Delta f = -20.8$ GHz and $\Delta f = 13.0$ GHz, respectively.

4. Conclusion

In summary, we experimentally demonstrate a method for simultaneously generating multi-channel broadband chaotic signals based on two unidirectional coupled WRC-FPLDs (M-WRC-FPLD and S-WRC-FPLD) with almost the same mode interval. The output of the free running M-WRC-FPLD is injected into the S-WRC-LD. Under suitable injection condition, multiple longitudinal modes of the S-WRC-LD can be driven into chaotic states, and then multi-channel chaotic signals can be generated simultaneously. Via a center wavelength tunable optical filter, the performances of 9-channel chaotic signals are inspected. The experiment results show that, under injection conditions ($\Delta f = -5$ GHz and $P_{\rm in} = 1.08$ mW, $\Delta f = 1$ GHz and $P_{\rm in} = 276.04$ μW, $\Delta f = 5$ GHz and $P_{\rm in} = 1.27$ mW) the chaotic bandwidths of the 9-channel chaotic signals are slightly different and locate within the range of 8$\sim$15 GHz, and the energy of each chaotic channel located at low-frequency region is stronger than that of the laser total chaotic output. For a given Δf, with the increase of injection power, the chaotic bandwidth for a determined channel shows a trend of increasing first and then decreasing. For a given $P_{\rm in}$, the variation of the chaotic bandwidth presents an approximately symmetrical m-shaped distribution for Δf varied within -30 GHz to 30 GHz. Due to the relatively simple structure and the ability to simultaneously generate, our proposed scheme is valuable for providing multi-channel chaotic sources for application in WDM chaotic optical communication and multi-channel high-speed random number generation.

Acknowledgment

The authors would like to thank the anonymous reviewers for their valuable suggestions.

References

[1] A. Uchida *et al.*, "Fast physical random bit generation with chaotic semiconductor lasers," *Nature Photon.*, vol. 2, no. 12, pp. 728–732, Nov. 2008.
[2] Y. Wang, S. Y. Xiang, B. Wang, X. Y. Cao, A. J. Wen, and Y. Hao, "Time-delay signature concealment and physical random bits generation in mutually coupled semiconductor lasers with FBG filtered injection," *Opt. Express*, vol. 27, no. 6, pp. 8446–8455, Mar. 2019.
[3] X. Tang *et al.*, "Fast physical random bit generation based on a broadband chaotic entropy source originated from a filtered feedback WRC-FPLD," *IEEE Photon. J.*, vol. 11, no. 2, Apr. 2019, Art. no. 7800710.
[4] Y. C. Wang, B. J. Wang, and A. B. Wang, "Chaotic correlation optical time domain reflectometer utilizing laser diode," *IEEE Photon. Technol. Lett.*, vol. 20, no. 19, pp. 1636–1638, Oct. 2008.
[5] D. Z. Zhong, Z. Z. Xiao, G. Z. Yang, N. Zhen, and H. Yang, "Real-time ranging of the six orientational targets by using chaotic polarization radars in the three-node VCSEL network," *Opt. Express*, vol. 27, no. 7, pp. 9857–9867, Apr. 2019.
[6] F. H. Shen, J. Jie, C. B. Xie, Z. Wang, and B. X. Wang, "High-spectra resolution Mie Doppler lidar based on a two-stage Fabry-Perot etalon for tropospheric wind and aerosol accurate measurement," *Appl. Opt.*, vol. 58, no. 9, pp. 2216–2225, Mar. 2019.
[7] F. Y. Lin and J. M. Liu, "Chaotic lidar," *IEEE J. Sel. Top. Quantum Electron.*, vol. 10, no. 5, pp. 991–997, Dec. 2004.
[8] J. P. Goedgebuer, P. Levy, L. Larger, C. C. Chen, and W. T. Rhodes, "Optical communication with synchronized hyperchaos generated electrooptically," *IEEE J. Quantum Electron.*, vol. 38, no. 9, pp. 1178–1183, Sep. 2002.
[9] A. Argyris *et al.*, "Chaos-based communications at high bit rates using commercial fiber-optic links," *Nature*, vol. 438, no. 7066, pp. 343–346, Dec. 2005.

[10] R. Lavrov, M. Jacquot, and L. Larger, "Nonlocal nonlinear electro-optic phase dynamics demonstrating 10 Gb/s chaos communications," *IEEE J. Quantum Electron.*, vol. 46, no. 10, pp. 1430–1435, Oct. 2010.
[11] M. F. Cheng *et al.*, "Security-enhanced OFDM-PON using hybrid chaotic system," *IEEE Photon. Technol. Lett.*, vol. 27, no. 3, pp. 326–329, Feb. 2015.
[12] C. P. Xue *et al.*, "Security-enhanced chaos communication with time-delay signature suppression and phase encryption," *Opt. Lett.*, vol. 41, no.16, pp. 3690–3693, Aug. 2016.
[13] J. X. Ke, L. L. Yi, G. Q. Xia, and W. S. Hu, "Chaotic optical communications over 100-km fiber transmission at 30-Gb/s bit rate," *Opt. Lett.*, vol. 43, no. 6, pp. 1323–1326, Mar. 2018.
[14] N. Jiang, A. Zhao, C. Xue, J. Tang, and K. Qiu, "Physical secure optical communication based on private chaotic spectral phase encryption/ decryption," *Opt. Lett.*, vol. 44, no.7, pp. 1536–1539, Apr. 2019.
[15] V. Kovanis, A. Gavrielides, T. B. Simpson, and J. M. Liu, "Instabilities and chaos in optically injected semiconductor lasers," *Appl. Phys. Lett.*, vol. 67, no. 19, pp. 2780–2782, Nov. 1995.
[16] Y. H. Hong, P. S. Spencer, and K. A. Shore, "Enhancement of chaotic signal bandwidth in vertical-cavity surface-emitting lasers with optical injection," *J. Opt. Soc. Amer. B*, vol. 29, no. 3, pp. 415–419, Mar. 2012.
[17] G. H. Yuan, X. Zhang, and Z. R Wang, "Chaos generation in a semiconductor ring laser with an optical injection," *Optik*, vol. 124, no. 22, pp. 5715–5718, Nov. 2013.
[18] J. Mork, B. Tromborg, and J. Mark, "Chaos in semiconductor lasers with optical feedback: Theory and experiment," *IEEE J. Quantum Electron.*, vol. 28, no. 1, pp. 93–108, Jan. 1992.
[19] A. B. Wang, Y. C. Wang, and H. C. He, "Enhancing the bandwidth of the optical chaotic signal generated by a semiconductor laser with optical feedback," *IEEE Photon. Technol. Lett.*, vol. 20, no. 19, pp. 1633–1635, Oct. 2008.
[20] K. Schires, S. Gomez, A. Gallet, G. H. Duan, and F. Grillot, "Passive chaos bandwidth enhancement under dual-optical feedback with Hybrid III–V/Si DFB laser," *IEEE J. Sel. Top. Quantum Electron.*, vol. 23, no. 6, pp. 1–10, Jul. 2017.
[21] F. Y. Lin and J. M. Liu, "Nonlinear dynamical characteristics of an optically injected semiconductor laser subject to optoelectronic feedback," *Opt. commun.*, vol. 221, pp. 173–180, Jun. 2003.
[22] K. E. Callan, L. Illing, Z. Gao, D. J. Gauthier, and E. Scholl, "Broadband chaos generated by an optoelectronic oscillator," *Phys. Rev. Lett.*, vol. 104, no.11, pp. 113901–113904, Mar. 2010.
[23] J. F. Liao and J. Q. Sun, "Polarization dynamics and chaotic synchronization in unidirectionally coupled VCSELs subjected to optoelectronic feedback," *Opt. Commun.*, vol. 295, pp. 188–196, May 2013.
[24] J. Paul, S. Sivaprakasam, and K. A. Shore, "Dual-channel chaotic optical communications using external-cavity semiconductor lasers," *J. Opt. Soc. Amer. B*, vol. 21, no.3, pp. 514–521, Mar. 2004.
[25] X. Tang *et al.*, "Generation of multi-channel high-speed physical random numbers originated from two chaotic signals of mutually coupled semiconductor lasers," *Laser Phys. Lett.*, vol. 12, no. 1, Jan. 2015, Art. no. 015003.
[26] S. Y. Xiang, B. Wang, Y. Wang, Y. N. Han, A. J. Wen, and Y. Hao, "2.24-Tb/s physical random bit generation with minimal post-processing based on chaotic semiconductor lasers network," *J. Lightw. Technol.*, vol. 37, no. 16, pp. 3987–3993, Aug. 2019.
[27] X. J. Yao, X. Tang, Z. M. Wu, and G. Q. Xia, "Multi-channel physical random number generation based on two orthogonally mutually coupled 1550 nm vertical-cavity surface-emitting lasers," *Acta Phys. Sin.*, vol. 67, no. 2, pp. 20420401–20420408, Jan. 2018.
[28] N. Jiang, C. P. Xue, Y. X. Lv, and K. Qiu, "Physically enhanced secure wavelength division multiplexing chaos communication using multimode semiconductor lasers," *Nonlinear Dyn.*, vol. 86, no. 3, pp. 1937–1949, Aug. 2016.
[29] P. Li *et al.*, "Observation of flat chaos generation using an optical feedback multi-mode laser with a band-pass filter," *Opt. Express*, vol. 27, no. 13, pp. 17859–17867, Jun. 2019.
[30] N. Q. Li, W. Pan, L. S. Yan, B. Luo, X. H. Zou, and S. Y. Xiang, "Enhanced two-channel optical chaotic communication using isochronous synchronization," *IEEE J. Sel. Top. Quantum Electron.*, vol. 19, no. 4, Jul. 2012, Art. no. 0600109.
[31] G. R. Lin, H. L. Wang, G. C. Lin, Y. H. Huang, Y. H. Lin, and T. K. Cheng, "Comparison on injection-locked Fabry–Perot laser diode with front-facet reflectivity of 1% and 30% for optical data transmission in WDM-PON system," *J. Lightw. Technol.*, vol. 27, no. 14, pp. 2779–2785, Apr. 2009.
[32] G. R. Lin, T. K. Cheng, Y. H. Lin, G. C. Lin, and H. L. Wang, "Suppressing chirp and power penalty of channelized ASE injection-locked mode-number tunable weak-resonant-cavity FPLD transmitter," *IEEE J. Quantum Electron.*, vol. 45, no. 9, pp. 1106–1113, Sep. 2009.
[33] Z. Q. Zhong *et al.*, "Tunable broadband chaotic signal synthesis from a WRC-FPLD subject to filtered feedback," *IEEE Photon. Technol. Lett.*, vol. 29, no. 17, pp. 1506–1509, Sep. 2017.
[34] S. Y. Lin, Y. C. Chi, Y. C. Su, Y. C. Li, and G. R. Lin, "An injection-locked weak-resonant-cavity laser diode for beyond-bandwidth encoded 10-Gb/s OOK transmission," *IEEE Photon. J.*, vol. 7, no. 1, Feb. 2015, Art. no. 7200309.